Author/s:
Setareh, M;De Gille, R;Cadusch, J;Wen, D;Kim, S;Crozier, KB

Title:
High Efficiency Triple-Helix Solenoid Beam Generated by Dielectric Metasurface

Date:
2024-09-18

Citation:
Setareh, M., De Gille, R., Cadusch, J., Wen, D., Kim, S. & Crozier, K. B. (2024). High Efficiency Triple-Helix Solenoid Beam Generated by Dielectric Metasurface. ACS Photonics, 11 (9), pp.3486-3491. https://doi.org/10.1021/acsphotonics.4c00874.

Persistent Link:
https://hdl.handle.net/11343/368889

High efficiency triple-helix solenoid beam generated by dielectric metasurface

MARYAM SETAREH,[1,2] ROBERT DE GILLE,[3] JASPER CADUSCH,[1] DANDAN WEN,[1,4] SEJEONG KIM,[1] AND KENNETH B. CROZIER[1,2,3*]

[1] *Department of Electrical and Electronic Engineering, University of Melbourne, Victoria 3010, Australia*
[2] *Australian Research Council Centre of Excellence for Transformative Meta-Optical System (TMOS), University of Melbourne, VIC 3010, Australia*
[3] *School of Physics, University of Melbourne, Victoria 3010, Australia*
[4] *School of Physical Science and Technology, Northwestern Polytechnical University, Xi'an 710129, China*
** kenneth.crozier@unimelb.edu.au*

ABSTRACT: Solenoid beams are structured beams exhibiting patterns of light that rotate around the axis of propagation. They can exert forces on objects in a direction opposite to the light propagation direction and are thus referred to as tractor beams. Previous studies have produced solenoid beams using spatial light modulators (SLMs), but cost, weight, and size limit their widespread application. Here, we experimentally demonstrate a silicon metasurface that generates a triple helix solenoid beam. The beam is equivalent to the superposition of Bessel beams with orbital angular momentum (OAM) values of -10 and -7 and internal angles of 0.005 and 0.004 rad, respectively. Our metasurface demonstrates a diffraction efficiency of >90% and a transmission of >75%, a significant improvement over SLMs. We map the beam's intensity profile at up to ~21 cm from the metasurface, showing its triple helix profile with negligible diffraction. We furthermore experimentally investigate interference between the solenoid beam and a Gaussian beam. This allows us to unravel the OAM information embedded in our two-component solenoid beam.

KEYWORDS: *solenoid beams, tractor beams, metasurfaces, interference patterns, optical forces*

INTRODUCTION

The momentum flux in optical beams leads to radiation pressure that generally pushes objects in the direction of the wavevector. Significant interest has recently been generated regarding beams that can instead pull objects in the opposite direction, i.e. toward the source. These are termed tractor beams. Various innovative methods have been explored. However, these pioneering works have confronted challenges related to beam quality, efficiency, and the need for modulation of the beam in time. We describe these next.

Ruffner et al. in 2012 introduced a tractor beam employing optical conveyors composed of two Bessel beams with different internal angles. However, the tractor beam functionality required the relative phase between the beams to be modulated in time [1]. In 2013, Kajorndejnukul et al. demonstrated the generation of a pulling force on 10 μm dodecane droplets (refractive index 1.42) at the air-water interface. They attributed this to the Minkowski form of electromagnetic momentum density within materials, in conjunction with the principle of momentum conservation [2]. Shvedov et al. (2014) demonstrated the use of azimuthally polarized light to pull gold-coated hollow glass spheres via photophoretic forces arising from a non-uniform temperature distribution, although specific particle characteristics were essential for its effectiveness [3]. Lee et al. proposed a solenoid beam with a negative helical pitch to create a negative scattering force for particle manipulation, albeit relying on spatial light modulators (SLMs) with associated limitations [4]. In 2016, Yevick et al. theorized a solenoid beam created through the superposition of two Bessel beams possessing OAM of -5 and -4, with internal angles of 0.418 and 0.627 radians, to draw 50 nm diameter silica particles toward the source [5]. Rodrigo et al. in 2022 demonstrated the pulling of silica particles using an SLM-generated helical beam [6]. These seminal studies collectively explored distinct optical methodologies for particle manipulation, each with its unique strengths and limitations.

Here, we generate a triple helix solenoid beam with a metasurface. This beam is engineered to exert a pulling force. We suggest that our approach has advantages over previous works. Unlike Ref. 1, it does not require time-modulation of the beam. Our method, unlike Ref. 2, is not limited by the requirement that the objects be situated at interfaces between different refractive indices. Unlike Ref. 3, it does not impose tight constraints on the object to be manipulated. Unlike Refs. 4 and 6, it does not require an SLM. Our approach is largely inspired by Ref. 5, but we demonstrate the beam experimentally and introduce an interferometric method to characterize it. Early parts of our work were presented at a conference [7], but are significantly extended here.

Our paper is structured as follows. We begin by designing the phase hologram that creates the solenoid beam. We describe electromagnetic simulations used to design the metasurface atoms (amorphous silicon (a-Si) pillars) to achieve the necessary geometric phase with high transmission efficiency. We design and fabricate the metasurface. We characterize it experimentally and compare the results to simulations. We map the beam intensity vs distance at up to ~21 cm from the metasurface. These experiments confirm that a triple helix beam with negligible diffraction is achieved. We implement an interferometric characterization method that is novel for these beams to the best of our knowledge. This involves us interfering the solenoid beam with a Gaussian beam. This results in interference patterns with intricate flower-like patterns. We show that from the number of spirals, the OAM values of the beams that constitute the solenoid beam can be determined. The paper concludes with a discussion of suggested areas of future work.

RESULTS AND DISCUSSION

We begin with a brief review of solenoid beams. These result from the superposition of Bessel beams with varying OAM and internal angles. They can be generated by as few as two Bessel beams [5]. If using bulk optical elements, each Bessel beam could be generated with an axicon

lens and a spiral phase plate (SPP). An axicon lens can be used to generate a zeroth order Bessel beam from a Gaussian beam, which can be in turn converted to a higher order Bessel beam with OAM using an SPP. The Bessel beam's non-diffracting property occurs within the axicon's depth of focus, requiring a smaller internal angle for longer-range beams.

When two Bessel beams, one with OAM of m and internal angle of α, and the other with OAM of n and internal angle of β, interfere to form a solenoid beam, the resulting beam's amplitude and phase at trap positions ($r=R$) are as follows [5]:

$$u(r)|_{r=R} = u_0 \cos\left(\frac{m-n}{2}\left[\theta - kz\frac{\cos\alpha-\cos\beta}{m-n}\right]\right) \quad (1)$$

$$\phi(r)|_{r=R} = \frac{m+n}{2}\theta + \frac{\cos\alpha+\cos\beta}{2}kz \quad (2)$$

Here, k is the wavenumber and z is the propagation direction. We aim to demonstrate a long-range solenoid, and thus choose constituent beams with very small internal angles. Two Bessel beams with OAM values of -10 and -7 and respective internal angles of 5 and 4 mrad are used. The condition for the OAM values and internal angles to create a solenoid tractor beam, as explained in Ref . 5, is that $n\cos(\alpha) > m\cos(\beta)$ (if $|m| > |n|$). Our solenoid beam satisfies this condition, indicating its potential as a tractor beam. We design our phase hologram to introduce an intentional tilt (of 9°) between the generated solenoid beam and the unconverted beam. This is done in anticipation of imperfections in the fabrication process, which would result in incomplete conversion of the beam. This tilt enables the desired beam to be spatially separated from the unconverted part.

We next discuss the metasurface used to generate the solenoid beam. Metasurfaces, consisting of subwavelength structures engineered to manipulate light, have emerged as powerful tools in optics, demonstrating versatility in various applications such as second and third harmonic generation [8–11], metalenses [12–15]and metaholograms [16–19]. Recently, metasurfaces have also been used to generate vortex beams, adding to their extensive range of capabilities [20–30]. Our metasurface is a Pancharatnam-Berry type (i.e. geometric phase) and based on a-Si nanopillar meta-atoms. Efficient incident beam phase modulation thus requires that the meta-atom should act like a halfwave plate [31,32]. A schematic illustration of the meta-atom is shown as Figure 1a. To determine the suitable dimensions (length L and width W) for these nanopillars, finite-element electromagnetic simulations are conducted using the commercial package COMSOL Multiphysics. These simulations are carried out at a wavelength of 1064 nm, as silicon exhibits low optical losses there. To calculate the conversion efficiency of the device, we consider the case in which the incident beam is x-polarized, with the nanofin oriented with θ = 45°. The conversion efficiency can then be found by Eq. 3,

$$\eta = \frac{|E_y|^2 - |E_x|^2}{|E_y|^2 + |E_x|^2} \quad (3)$$

where E_x and E_y are the electric field components along the x and y directions. We vary (L, W) systematically at a fixed height (H=505 nm) to maximize conversion efficiency and transmission. We find that the following dimensions give good results: (L, W)=(305 nm, 130 nm). We

choose a periodicity (Px=Py) of 430 nm.

The phase hologram that generates our triple helix solenoid beam with a deflection angle of 9° is shown as Figure 1b. It has an overall extent of 2.5 mm by 2.5 mm. The phase angles of this design (Fig. 1a) directly determine the orientation angles of the nanopillars in the metasurface. With these determined, we fabricate the metasurface. Fabrication starts with the deposition of a-Si onto a borosilicate glass substrate by plasma-enhanced chemical vapor deposition (Oxford Instruments). We then perform electron beam lithography (Vistec EBPG5000plusES). After development, electron beam evaporation of chromium (thickness: 30 nm) is carried out, and the lift-off process is performed. The device is completed using inductively coupled reactive ion etching (Oxford Instruments). An optical microscope image of the central part of the metasurface (overall extent $2.5 \times 2.5\ mm$) is shown as Figure 1c.

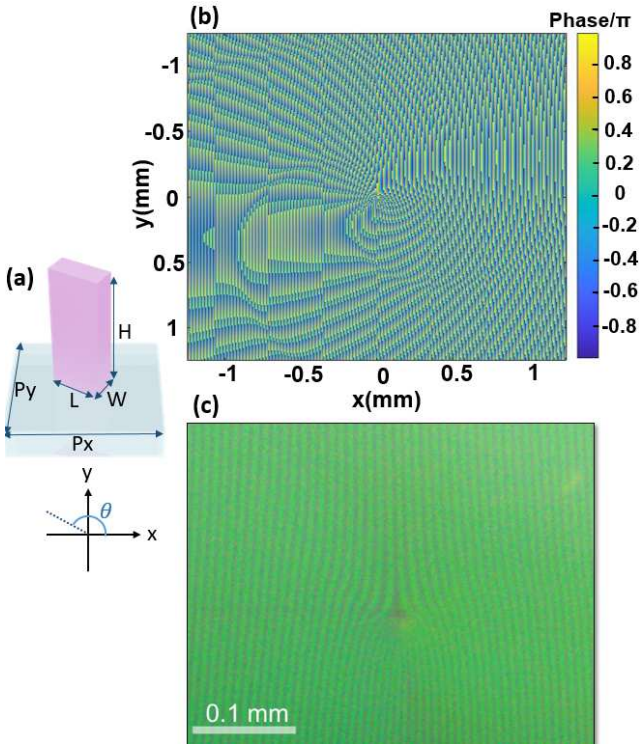

Figure 1(a) Schematic of meta-atom, comprising a-Si nanopillar, the building block of the metasurface, (b) Phase hologram required for generating solenoid beam with deflection angle of 9°. (c) Bright-field image of fabricated metasurface.

We test the efficiency of our metasurface as follows. We illuminate the metasurface with a right circularly polarized (RCP) Gaussian beam (beam width ~ 3 mm) at wavelength $\lambda = 1064\ nm$. This generates our triple helix solenoid beam at an angle of 9°, which corresponds to the +1 diffraction order. We measure the transmitted optical power. This allows us to determine the transmission of the hologram to be ~76%. Diffraction efficiencies are measured to be (~1%, ~6%, ~93%) for the (-1,0,+1) orders. We thus conclude that ~70% of the total input laser power goes into the desired beam, with ~24% being lost to the combination of reflection, scattering, and absorption, and ~5% going into the 0 and -1 orders.

A. Solenoid Beam Spatial Profile

We next experimentally assess the performance of the metasurface at generating the solenoid beam. We began by measuring the intensity profile at varying distances from the metasurface.

A schematic of the experimental set-up is shown as Fig. 2a. Light from an Nd:YAG laser (CNI Laser, $\lambda = 1064\ nm$) is coupled into a single mode optical fiber to ensure good beam quality. Light from the fiber is collimated with a lens (Thorlabs adjustable fiber collimator, f=11mm), passed through a linear polarizer (LP) and quarter waveplate (QWP). The resultant circularly polarized light then illuminates the metasurface (MS). As discussed, this generates a solenoid beam, whose handedness is opposite that of the illuminating beam, at a deflection angle of 9°. To measure the intensity profile, we use a complementary metal oxide semiconductor (CMOS) camera mounted on a long-travel motorized stage. The solenoid beam directly illuminates the image sensor (i.e. with no intervening lenses). In Fig. 2 (b-d) and (e-g), we show simulation and experimental results at three distances from the metasurface (3 cm, 5.6 cm, and 9cm). From these images, three intensity maxima can be seen. The presence of three peaks can be attributed to the difference between the OAM of the constituent Bessel beams. It can be seen that, as the beam propagates, it maintains its profile. We use the commercial software package MATLAB to analyze the data. Using MATLAB's "cpselect" tool and "fitgeotrans" function to analyze the simulation data, we observe a ~120.405° rotation over 13 cm, meaning that the rotation period for the three intensity maxima is ~38.9 cm. Applying the same method to the experimental data, we find a rotation period of ~38.6 cm.

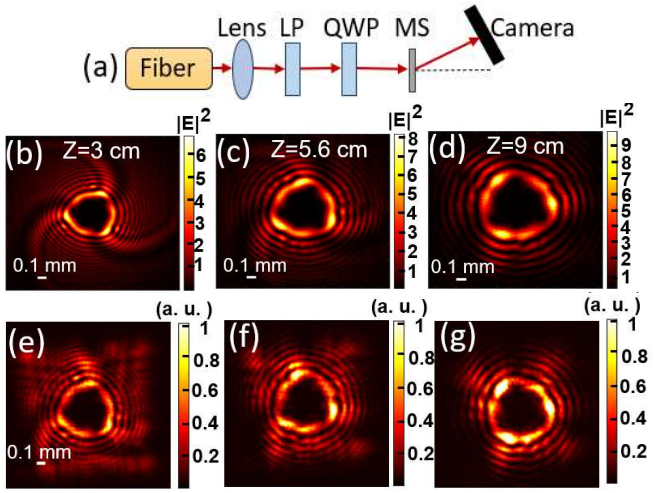

Figure 2 (a) Schematic of experimental setup used for capturing the beam intensity profile at different distances. Beam intensity profile at various distances from the metasurface: (b)-(d) simulation results for z=3cm, 5.6cm, and 9cm, (e)-(g) corresponding experimental results.

We next plot the experimental results as a volumetric intensity profile over a distance range of 2 cm to 21 cm from the metasurface (Fig. 3 (a)). The triple helix pattern can again be clearly seen. In Fig. 3 (b), the corresponding theoretical three-dimensional intensity distribution is plotted. This is produced using scalar diffraction theory, with calculations performed in MATLAB. These plots represent isosurfaces at 60% of the peak intensity. It can be seen that the measured intensity profile is in good agreement with theory, in terms of both the presence of three

spirals propagating around the optical axis and the fact that over this distance, the solenoid beam propagates with little diffraction.

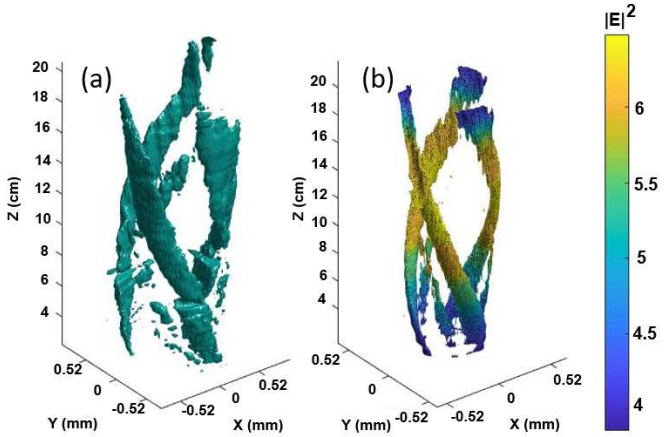

Figure 3 (a) Measured 3D intensity of triple-helix solenoid beam generated by metasurface. (b) Theoretical volumetric intensity of triple-helix solenoid beam.

B. Interference pattern

We next show that an interferometric method can yield further information on the solenoid beam, revealing the OAM values of the components. Evaluating OAM values typically requires interference setups that display specific spiral or forked patterns [33–37]. While many studies have outlined methods for measuring the characteristics of single-component vortex beams, there's a limited exploration into OAM within more complex beams.

Figures 4 (a1-b1) display the simulated intensity profiles of two different solenoid beams, calculated at a distance of 4 cm from the hologram generating them. In Figures 4 (a2-b2), the resulting simulated interference patterns from the interaction of these beams with a reference Gaussian beam are depicted. Analysis of both the interference patterns and intensity profiles facilitates the measurement of OAM. From analysis of various solenoid beams comprising Bessel beams with different orders, we find that the number of spirals within the interference patterns gives the OAM magnitude for one of the constituent Bessel beams. Meanwhile, for the other constituent beam, its OAM magnitude can be derived by assessing the intensity profile, with the number of intensity maxima corresponding to the OAM difference between the two beams [5]. Thus, subtracting the number of intensity maxima from the counted spirals provides the OAM magnitude of the second beam. This approach is verified for the beams Fig. 4 (a1- a2) and (b1-b2) as follows. For Fig. 4 (a1-a2), the constituent beams have $m = -8$ and $n = -3$. From the interference pattern (Fig. 4a2), it can be seen that eight spirals are present. We therefore have $|m| = 8$. From the intensity pattern (Fig. 4a1), it can be seen that there are five maxima. We therefore have $|n| = 3$, as expected. We next consider the beam of Fig. 4 (b1-b2), which has $m = -11$ and $n = -4$. From Fig. 4b2, 11 spirals can be seen, so we have $|m| = 11$. From Fig. 4b1, seven intensity maxima occur, so we have $|n| = 4$, as required. Curved white lines in Fig. 4 (b2) are included to assist visualization of the spiral counting process.

To apply this method, we perform interference measurements following the methodology employed in Ref. 38. In our experimental set-up (Fig. 4 (c)), a circularly polarized beam is divided with a beam splitter (BS). The upper-path beam traverses

the metasurface (MS), transforming into a solenoid beam, while the lower-path beam serves as the reference. The subsequent recombination of these beams by a second beam splitter yields the interference pattern.

In Figure 4 (d-e), we present the experimental and simulated results, respectively, for our interference method. It can be seen that both experiment and simulation reveal the presence of ten distinct spirals. We therefore have $|m| = 10$. From Figs. 2 and 3, we know that there are three intensity maxima. We therefore have $|n| = 7$. Our method therefore correctly predicts the magnitude of the OAM components of our solenoid beam.

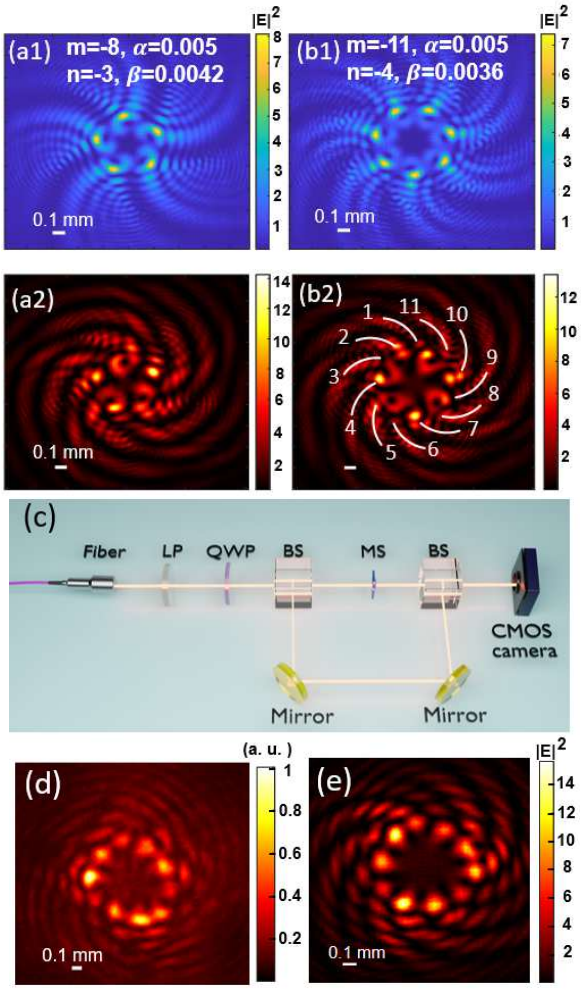

Figure 1 (a1-b1) Intensity profile of solenoid beams generated by Bessel beam with the OAMs of "m" and "n", and internal angles of α and β, respectively. (a2-b2) Corresponding interference patterns. (c) Schematic of the experimental interference setup (graphics adapted from Ref. 39), (d) Experimental result, and (e) simulation result of interference pattern for the triple-helix solenoid beam

CONCLUSION

We present an a-Si-based metasurface that generates a triple helix solenoid beam. A circularly polarized beam passing through the metasurface is converted to a solenoid beam with the opposite handedness. The intensity profiles are measured as a function of distance from the metasurface, demonstrating that the solenoid beam exhibits negligible diffraction over a substantial propagation distance. Our device has

a transmission efficiency of ~76% which, along with the small size, weight, and cost of the metasurface approach, render it as a promising alternative to SLM-based systems for a range of applications. We also show that an interferometric method that, in combination with the intensity profile, uncovers the OAM values of the constituent components, we note that the constituent beams composing the solenoid beam satisfy the necessary conditions for generating a tractor beam. As a result, we anticipate that the generated solenoid beam will exert a pulling force on particles within its path and that such metasurfaces may become important tools in the field of optical manipulation.

Funding. This work was supported in part by the Australian Research Council (ARC) Centre of Excellence for Transformative Meta-Optical Systems (Project ID CE200100010). This work was supported in part by the Melbourne Centre for Nanofabrication (MCN) Technology Fellow Ambassador program.

Acknowledgments. This work was performed in part at the MCN in the Victorian Node of the Australian National Fabrication Facility (ANFF).

Disclosures. The authors declare no competing financial interests.

Data availability. Data may be obtained from the authors upon reasonable request.

References

(1) Ruffner, D. B.; Grier, D. G. Optical Conveyors: A Class of Active Tractor Beams. *Phys Rev Lett* **2012**, *109* (16), 163903.
(2) Kajorndejnukul, V.; Ding, W.; Sukhov, S.; Qiu, C. W.; Dogariu, A. Linear Momentum Increase and Negative Optical Forces at Dielectric Interface. *Nat Photonics* **2013**, *7* (10), 787–790.
(3) Shvedov, V.; Davoyan, A. R.; Hnatovsky, C.; Engheta, N.; Krolikowski, W. A Long-Range Polarization-Controlled Optical Tractor Beam. *Nat Photonics* **2014**, *8* (11), 846–850.
(4) Lee, S.-H.; Roichman, Y.; Grier, D. G. Optical solenoid beams, *Optics express* **2010**, 18 (7), 6988-6993.
(5) Yevick, A.; Ruffner, D. B.; Grier, D. G. Tractor Beams in the Rayleigh Limit. *Phys Rev A* **2016**, *93* (4), 043807.
(6) Rodrigo, J. A.; Martínez-Matos, Ó.; Alieva, T. Helix-Shaped Tractor and Repulsor Beams Enabling Bidirectional Optical Transport of Particles En Masse. *Photonics Res* **2022**, *10* (11), 2560-2574.
(7) Cadusch, J.; Wen, D.; Meng, J.; Crozier, K. B. *Triple-Helix Tractor Beam Generation with a Dielectric Metasurface Pancharatnam-Berry Phase Hologram*; *Conference on Lasers and Electro-Optics (CLEO)* **2021**, 1-2.
(8) Reineke, B.; Sain, B.; Zhao, R.; Carletti, L.; Liu, B.; Huang, L.; De Angelis, C.; Zentgraf, T. Silicon Metasurfaces for Third Harmonic Geometric Phase Manipulation and Multiplexed Holography. *Nano Lett* **2019**, *19* (9), 6585–6591.
(9) Liu, B.; Geromel, R.; Su, Z.; Guo, K.; Wang, Y.; Guo, Z.; Huang, L.; Zentgraf, T. Nonlinear Dielectric Geometric-Phase Metasurface with Simultaneous Structure and Lattice Symmetry Design. *ACS Photonics* **2023**, *10* (12), 4357–4366.
(10) Keren-Zur, S.; Avayu, O.; Michaeli, L.; Ellenbogen, T. Nonlinear Beam Shaping with Plasmonic Metasurfaces. *ACS Photonics* **2016**, *3* (1), 117–123.
(11) Mekhael, M.; Stolt, T.; Vesala, A.; Rekola, H.; Hakala, T. K.; Fickler, R.; Huttunen, M. J. Phase-Matched Second-Harmonic Generation from Metasurfaces Inside Multipass Cells. *ACS Photonics* **2024**, *11* (2), 682–687.
(12) Barulin, A.; Kim, Y.; Oh, D. K.; Jang, J.; Park, H.; Rho, J.; Kim, I. Dual-Wavelength Metalens Enables Epi-Fluorescence Detection from Single Molecules. *Nat Commun* **2024**, *15* (1), 26.
(13) Arbabi, E.; Arbabi, A.; Kamali, S. M.; Horie, Y.; Faraji-Dana, M. S.; Faraon, A. MEMS-Tunable Dielectric Metasurface Lens. *Nat Commun* **2018**, *9* (1), 812.
(14) Geromel, R.; Rennerich, R.; Zentgraf, T.; Kitzerow, H. Geometric-Phase Metalens to Be Used for Tunable Optical Tweezers in Microfluidics. *Liq Cryst* **2023**, *50* (7–10), 1193–1203.
(15) Chantakit, T.; Schlickriede, C.; Sain, B.; Meyer, F.; Weiss, T.; Chattham, N.; Zentgraf, T. All-Dielectric Silicon Metalens for Two-Dimensional Particle Manipulation in Optical Tweezers. *Photonics Res* **2020**, *8* (9), 1435-1440.
(16) Wan, W.; Gao, J.; Yang, X. Full-Color Plasmonic Metasurface Holograms. *ACS Nano* **2016**, *10* (12), 10671–10680.
(17) Frese, D.; Wei, Q.; Wang, Y.; Cinchetti, M.; Huang, L.; Zentgraf, T. Nonlinear Bicolor Holography Using Plasmonic Metasurfaces. *ACS Photonics* **2021**, *8* (4), 1013–1019.
(18) Wen, D.; Yue, F.; Li, G.; Zheng, G.; Chan, K.; Chen, S.; Chen, M.; Li, K. F.; Wong, P. W. H.; Cheah, K. W.; Yue Bun Pun, E.; Zhang, S.; Chen, X. Helicity Multiplexed Broadband Metasurface Holograms. *Nat Commun* **2015**, *6 (1), 8241*.

(19) Zheng, G.; Mühlenbernd, H.; Kenney, M.; Li, G.; Zentgraf, T.; Zhang, S. Metasurface Holograms Reaching 80% Efficiency. *Nat Nanotechnol* **2015**, *10* (4), 308–312.
(20) Chen, M. H.; Chen, B. W.; Xu, K. L.; Su, V. C. Wide-Angle Optical Metasurface for Vortex Beam Generation. *Nanomaterials* **2023**, *13* (19), 2680.
(21) Shen, Z.; Li, R.; Xue, Y. Z.; Qiu, Z. Y.; Xiang, Z. Y.; Zhou, J. Y.; Zhang, B. F. Generation of Optical Vortices with Polarization-Insensitive Metasurfaces. *IEEE Photonics J* **2020**, *12* (4), 1-10.
(22) Su, V. C.; Chiang, C. H.; Chen, M. H.; Xu, K. L.; Huang, S. Y. Metasurface-Based Perfect Vortex Beam for Optical Eraser. *Commun Phys* **2024**, *7* (1), 36.
(23) Chen, Q.; Liu, P.; Fu, Y.; Zhang, S.; Zhang, Y.; Yuan, X.; Min, C. Monolayer Chiral Metasurface for Generation of Arbitrary Vector Beams **2024,** 11(1), 57.
(24) Colburn, S.; Majumdar, A.; Majumdar, A. Metasurface Generation of Paired Accelerating and Rotating Optical Beams for Passive Ranging and Scene Reconstruction. *ACS Photonics* **2020**, *7* (6), 1529–1536.
(25) Zhang, C.; Yue, F.; Wen, D.; Chen, M.; Zhang, Z.; Wang, W.; Chen, X. Multichannel Metasurface for Simultaneous Control of Holograms and Twisted Light Beams. *ACS Photonics* **2017**, *4* (8), 1906–1912.
(26) Chen, S.; Cai, Y.; Li, G.; Zhang, S.; Cheah, K. W. Geometric Metasurface Fork Gratings for Vortex-Beam Generation and Manipulation. *Laser Photon Rev* **2016**, *10* (2), 322–326.
(27) Yang, Y.; Wang, W.; Moitra, P.; Kravchenko, I. I.; Briggs, D. P.; Valentine, J. Dielectric Meta-Reflectarray for Broadband Linear Polarization Conversion and Optical Vortex Generation. *Nano Lett* **2014**, *14* (3), 1394–1399.
(28) Liang, C.; Dai, Q.; Huang, T.; Liu, H. C.; Guan, Z.; Fu, R.; Tao, J.; Li, Z.; Yu, S.; Zheng, G. Single-Celled Metasurface for Labeled Vortex Beam Generator. *Journal of Materiomics* **2024**, 10 (4), 811-818
(29) Devlin, R. C.; Ambrosio, A.; Rubin, N. A.; Mueller, J. P. B.; Capasso, F. *Arbitrary Spin-to-Orbital Angular Momentum Conversion of Light*. *Science* **2017**, 358 (6365), 896-901
(30) Ahmed, H.; Intaravanne, Y.; Ming, Y.; Ansari, M. A.; Buller, G. S.; Zentgraf, T.; Chen, X. Multichannel Superposition of Grafted Perfect Vortex Beams. *Advanced Materials* **2022**, *34* (30), 2203044
(31) Ni, P. N.; Fu, P.; Chen, P. P.; Xu, C.; Xie, Y. Y.; Genevet, P. Spin-Decoupling of Vertical Cavity Surface-Emitting Lasers with Complete Phase Modulation Using on-Chip Integrated Jones Matrix Metasurfaces. *Nat Commun* **2022**, *13* (1), 7795.
(32) Zeng, J.; Dong, Y.; Zhang, J.; Wang, J. Broadband and High-Efficiency Multi-Tasking Silicon-Based Geometric-Phase Metasurfaces: A Review. *Photonics* **2022**, 9(9), 606.
(33) Maguid, E.; Chriki, R.; Yannai, M.; Kleiner, V.; Hasman, E.; Friesem, A. A.; Davidson, N. Topologically Controlled Intracavity Laser Modes Based on Pancharatnam-Berry Phase. *ACS Photonics* **2018**, *5* (5), 1817–1821.
(34) Tan, H.; Deng, J.; Zhao, R.; Wu, X.; Li, G.; Huang, L.; Liu, J.; Cai, X. A Free-Space Orbital Angular Momentum Multiplexing Communication System Based on a Metasurface. *Laser Photon Rev* **2019**, *13* (6), 1800278.
(35) Liu, X.; Deng, J.; Jin, M.; Tang, Y.; Zhang, X.; Li, K. F.; Li, G. Cassegrain Metasurface for Generation of Orbital Angular Momentum of Light. *Appl Phys Lett* **2019**, *115* (22).
(36) Gui, L.; Wang, C.; Ding, F.; Chen, H.; Xiao, X.; Bozhevolnyi, S. I.; Zhang, X.; Xu, K. 60 Nm Span Wavelength-Tunable Vortex Fiber Laser with Intracavity Plasmon Metasurfaces. *ACS Photonics* **2023**, 10(3), 623-631.
(37) Wang, H.; Wang, H.; Ruan, Q.; Chan, J. Y. E.; Zhang, W.; Liu, H.; Rezaei, S. D.; Trisno, J.; Qiu, C. W.; Gu, M.; Yang, J. K. W. Coloured Vortex Beams with Incoherent White Light Illumination. *Nat Nanotechnol* **2023**, *18* (3), 264–272.
(38) Dorrah, A. H.; Rubin, N. A.; Tamagnone, M.; Zaidi, A.; Capasso, F. Structuring Total Angular Momentum of Light along the Propagation Direction with Polarization-Controlled Meta-Optics. *Nat Commun* **2021**, 12 (1), 6249.
(39) Optical components pack v1. https://ryomizutagraphics.gumroad.com/l/OpticalComponentsV1 (Accessed 2024-07-11).

For Table of Contents Use Only

Title: High efficiency triple-helix solenoid beam generated by dielectric metasurface

Names of authors: Maryam Setareh, Robert De Gille, Jasper Cadusch, Dandan Wen, Sejeong Kim, and Kenneth B. Crozier

Brief synopsis describing the graphic: The graphic illustrates the process of generating a triple helix solenoid beam using a metasurface. A laser beam (λ=1064 nm) emerging from a fiber collimator passes through a linear polarizer and a quarter wave plate to generate circularly polarized light. The latter passes through the metasurface and is transformed into a triple helix solenoid beam.